applied sciences

MDPI

Article

The Influence of Chamfered and Rounded Corners on Vortex-Induced Vibration of Super-Tall Buildings

Lei Wang and Wei Zhang *

School of Civil Engineering, Henan Polytechnic University, Jiaozuo 454000, China
* Correspondence: zhangwei94818@163.com

Abstract: In order to study the influence of chamfered and rounded corners on vortex-induced vibration of super-tall buildings, a series of multi-degree-of-freedom (MDOF, in short) aeroelastic models were made, including chamfered-corner models with chamfer ratios of 0%, 2.5%, 5.0%, 7.5%, and 12.5%, and rounded-corner models with rounded ratios of 0%, 12.5%, 15%, and 17.5%. The crosswind displacement response of each aeroelastic model was measured by a laser displacement meter in a wind tunnel. The test results indicate that the crosswind displacement response is significantly reduced when the chamfer ratio increases to 5% or the rounded ratio increases to 12.5%; in particular, the vortex-induced vibration (VIV, in short) response can be reduced by more than 60%, which indicates that the chamfered corner and rounded corner play a good role in restraining the VIV of super high-rise buildings. When the reduced wind speed is small, the reduction of the crosswind response of chamfered and rounded models is mainly caused by the reduction of wind load; when the reduced wind speed approaches the VIV wind speed, the negative aerodynamic damping phenomenon of the model with a proper chamfer ratio and rounded ratio disappears, which shows that the VIV is suppressed not only because the cut corner reduces the wind load but also because the cut corner weakens the aeroelastic effect. Generally speaking, a chamfer ratio of about 7.5% and rounded ratio of about 15% can achieve a good reduction effect on the VIV of super high-rise buildings.

Keywords: tall buildings; vortex-induced vibration; MDOF aeroelastic model; chamfered-corner; rounded-corner

check for updates

Citation: Wang, L.; Zhang, W. The Influence of Chamfered and Rounded Corners on Vortex-Induced Vibration of Super-Tall Buildings. *Appl. Sci.* **2023**, *13*, 1049. https://doi.org/10.3390/app13021049

Academic Editor: Edyta Plebankiewicz

Received: 18 November 2022
Revised: 29 December 2022
Accepted: 5 January 2023
Published: 12 January 2023

Copyright: © 2023 by the authors. Licensee MDPI, Basel, Switzerland. This article is an open access article distributed under the terms and conditions of the Creative Commons Attribution (CC BY) license (https://creativecommons.org/licenses/by/4.0/).

1. Introduction

The current shift towards increasingly tall and slender buildings is likely to result in excessive structural vibrations when the buildings are subjected to strong winds, especially vibrations caused by vortexes in the crosswind direction. As is known, vortex-induced vibration may occur when the vortex shedding frequency approaches the natural frequency of a flexible structure, which is usually much more significant than the along-wind response [1–11].

Modification of aerodynamic shape can significantly reduce the wind-induced response of wind-sensitive structures (tall buildings, etc.). Many researchers have studied the influence of building shape on the wind-induced responses or wind load of tall buildings. As early as the 1980s, Kwok et al. [12] carried out a series of single-degree-of-freedom (SDOF, in short) aeroelastic model wind tunnel tests and found that the chamfered corner with a 10% chamfer ratio can reduce the crosswind and along-wind displacement by 30~40%. Kawai et al. [13] carried out SDOF aeroelastic model tests on cylinders with various cut corners. Kawai's research shows that even if the corner size changes only by 5% of the cross-section, the wind-induced response will still be greatly affected. Hayashida studied the influence of different section shapes on the wind force and wind pressure of super high-rise buildings using high-frequency force balance and a synchronous pressure model [14,15]. Gu et al. [16], Miyashita et al. [17], and Tanaka et al. [18]. analyzed the

wind load of super high-rise buildings with various sections through high-frequency force balance tests. Zhang et al. [19], on the other hand, studied the wind load of square column models with chamfered and rounded corners through the wind tunnel experiment of high-frequency force balance. Tamura et al. [20] carried out many experiments to study the influence of various building shapes on wind load by high-frequency force balance and rigid pressure model test. In addition to the above research, a large number of researchers have studied building shape modification through wind tunnel tests or CFD simulation [21–25].

Although many researchers have studied the influence of the chamfered corner and rounded corner on the wind effects of super high-rise buildings, most existing studies are carried out by using rigid pressure models and force balance tests. As is well known, the rigid pressure model and force balance test cannot take into account the influence of aeroelastic effects, while the aeroelastic model, especially the MDOF aeroelastic model test, is an accurate way to simulate wind-induced response and aeroelastic effect. Due to this reason, a series of MDOF aeroelastic model tests were carried out in this study to investigate the influence of the chamfered corner and rounded corner on VIV and obtain some conclusions that can provide guidance for the selection of body shape for super high-rise buildings.

2. Aeroelastic Model Skeleton and Wind Tunnel Test

2.1. Design of MDOF Model Skeleton

The research object of this paper is a hypothetical high-rise building with a height of 600 m and a square cross-section. The building has an aspect ratio of 10 and a primary frequency of about 0.095 Hz. The test model is the MDOF aeroelastic model. A length scale of 1:600 was adopted, the scale ratio of vibration frequency is 100:1, and the scale ratio of wind velocity is 1:6 according to similarity theory.

The MDOF model skeleton is composed of six rigid plates and five elastic columns, all of which are made of aluminum alloy-6061 (as seen in Figure 1a). The thick central column is a standard square column, which was fixed at the center of the six rigid plates. At each side are four thin specifically shaped columns that can be moved horizontally to adjust the mode shape and stiffness (see Figure 1b). In this way, the sway frequency and torsion frequency—including the sway mass and moment of inertia, as well as the sway stiffness and rotational stiffness—can be easily adjusted to meet the requirements of a similar ratio at the same time. The rigid plate is a specifically shaped plate with a thickness of 10 mm (see Figure 1c,f). In order to control the moving accuracy of the thin columns, several positioning convex blocks were fitted into the rigid plate, while fixtures made of organic glass were used to connect the columns and rigid plates. In addition, these convex blocks can fit snugly into the holes of four thin columns. Several vertical and horizontal screw holes on the rigid plates can be used to fix the additional mass of blocks and the outer-skin plate, respectively. The bottom plate is shown in Figure 1d,g. There are five square holes in the bottom plate (see Figure 1d). The intermediate thick column and the surrounding thin column can be inserted into these holes snugly, and bolts can then fasten the columns and the bottom plate together. After the model skeleton is completed in accordance with the aforementioned method, the segmented outer-skin plate can then be put on the model skeleton to simulate the body shape of the structure (see Figure 1h). Figure 1i shows the sway and torsion mode shapes calculated using finite element software ANSYS 17.0 (FEM, in short), which considered the influence of the outer-skin plate on the mass distribution of the aeroelastic model. The mode shapes in Figure 1i indicate the first sway mode and second sway mode shape, respectively. The first sway mode derived from FEM and free vibration test is shown in Figure 1j.

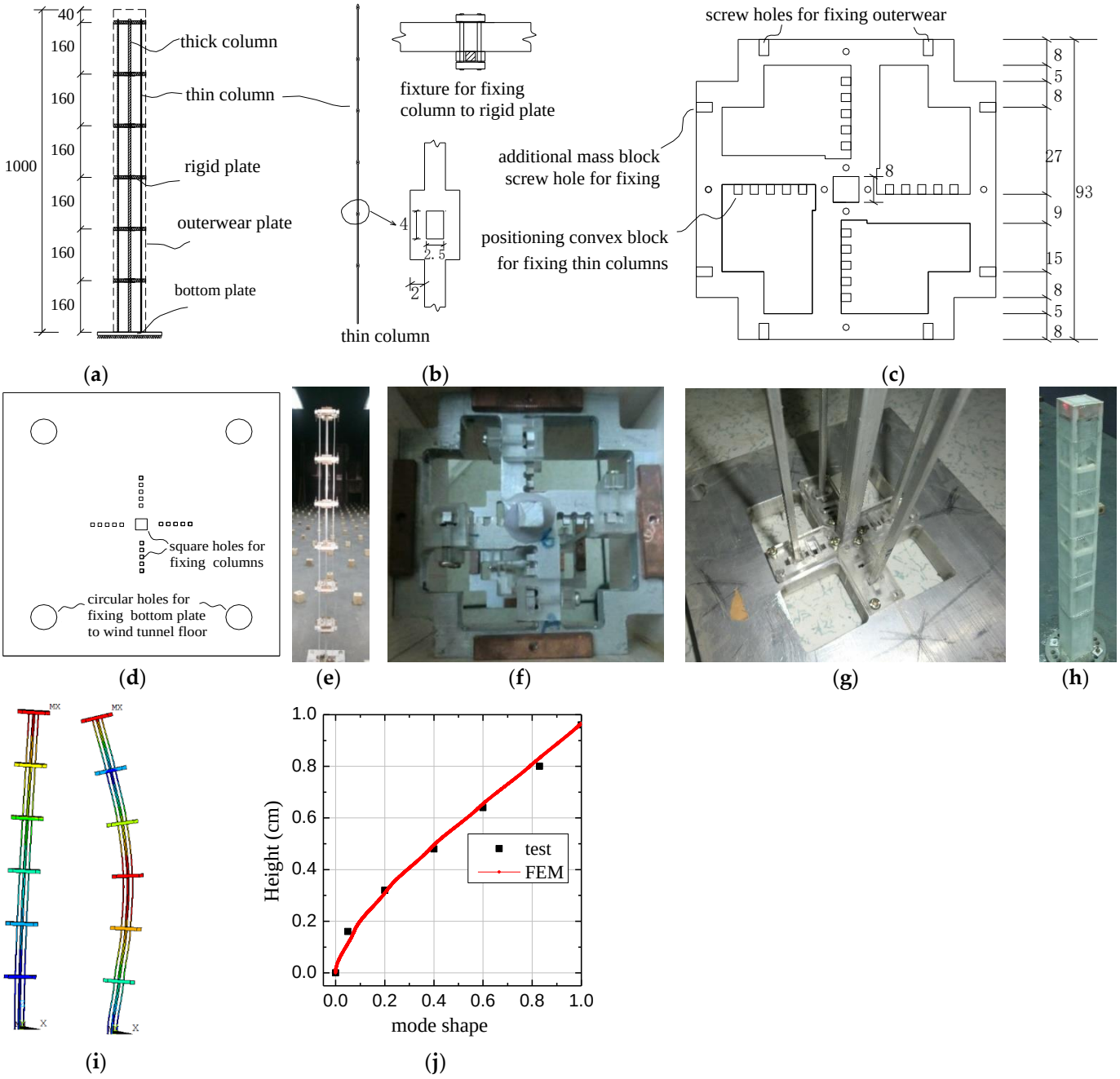


Figure 1. Design of the MDOF (unit: mm): (**a**) design of skeleton; (**b**) design of column and fixture; (**c**) design of rigid plate; (**d**) design of bottom plate; (**e**) skeleton photo; (**f**) photo of rigid plate; (**g**) photo of bottom plate; (**h**) completed model; (**i**) mode shapes of the completed model; (**j**) first sway mode shape derived from FEM and free vibration test.

2.2. Wind Tunnel Test

The wind tunnel test was conducted in the boundary layer wind tunnel of Wuhan University, China. The cross-section of the wind tunnel is 3.2 m wide × 2.1 m high. The wind speed in this wind tunnel can be continuously adjusted in the range of 0~30 m/s. The ground roughness was simulated using a set of spires and roughness elements upwind of building models. The aerodynamic contour and simulated turbulent wind field of the wind tunnel are shown in Figure 2, where the power-law 0.15 means the terrain category B in China's Code [26].

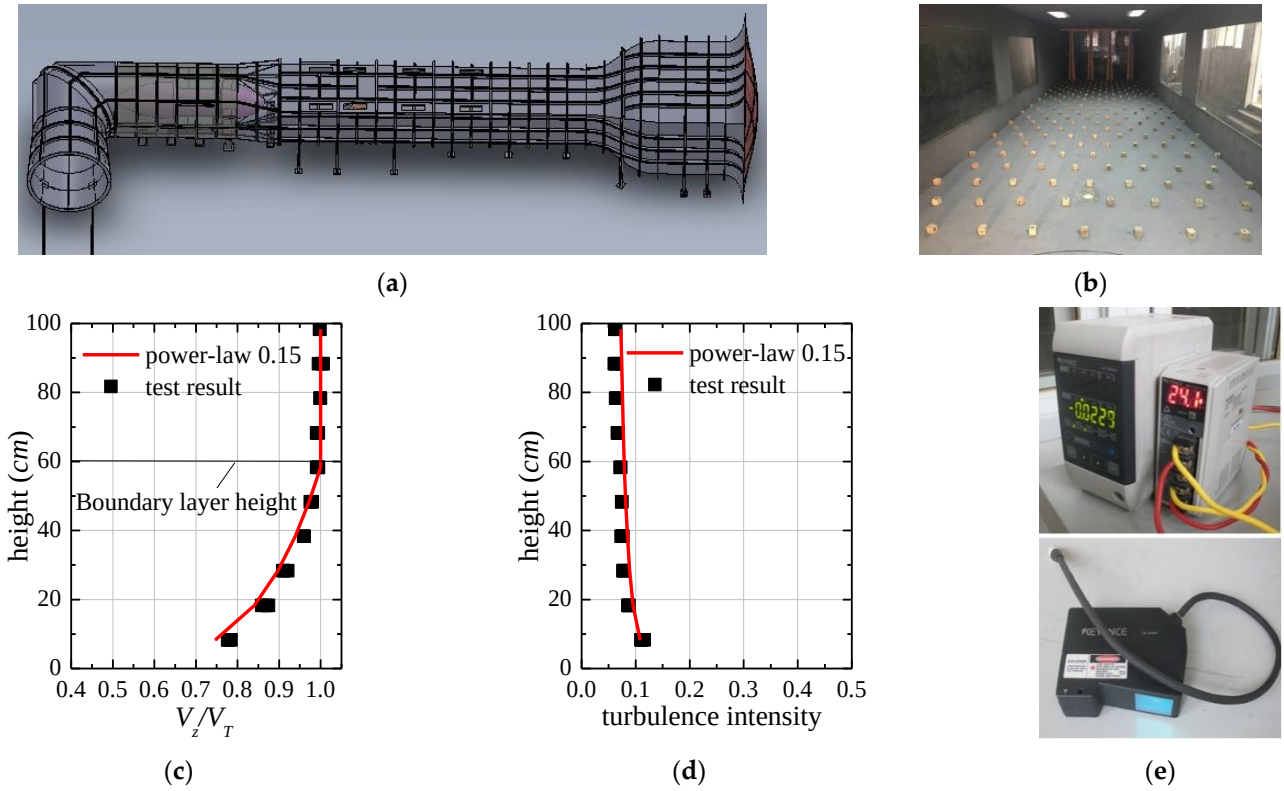


Figure 2. Wind tunnel and measuring instrument of this study: (**a**) aerodynamic contour of the wind tunnel; (**b**) simulation of the wind field; (**c**) mean wind velocity; (**d**) turbulence intensity; (**e**) laser displacement meter.

For all of the test cases of this study, the displacement response of the models was measured by a laser displacement meter (See Figure 2e); its sampling frequency is 500 Hz, and the test wind speed at the top of the aeroelastic model is about 4~16 m/s, and the corresponding Reynolds number is about 2.7×10^4–1.1×10^5.

3. Reduction Effect of Chamfered Corner on VIV

Aeroelastic Model with Chamfered Corner

Figure 3 shows the cross-sectional diagram of the chamfered-corner model. The chamfer ratio is 0%, 2.5%, 5%, 7.5%, and 12.5% successively, where the chamfer ratio is defined as the ratio of the chamfer size of one corner to the cross-sectional width. Considering the time and economic costs, the model skeleton was repeatedly used and the chamfer ratios were adjusted by the corresponding shapes of strips (See Figure 4). There is a red laser spot near the top of the model in Figure 4, which is the measured height of the wind-induced displacement.

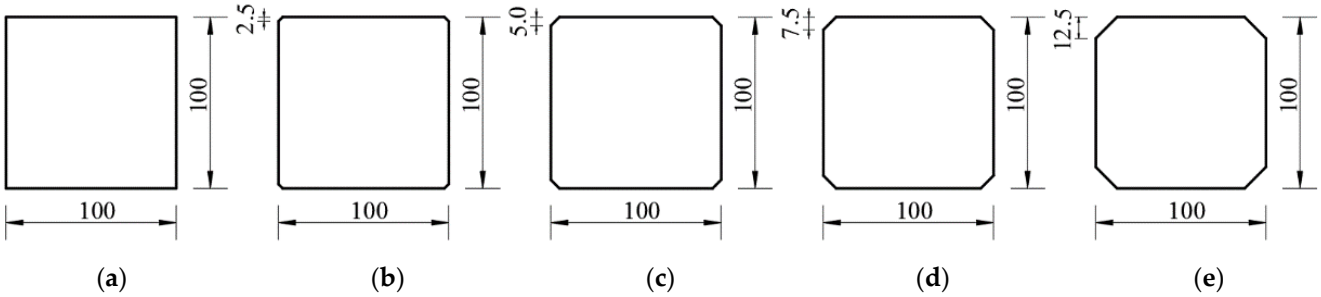


Figure 3. Cross-sections of MDOF model with chamfered corner (unit: mm): (**a**) chamfer ratio 0%; (**b**) chamfer ratio 2.5%; (**c**) chamfer ratio 5%; (**d**) chamfer ratio 7.5%; (**e**) chamfer ratio 12.5%.

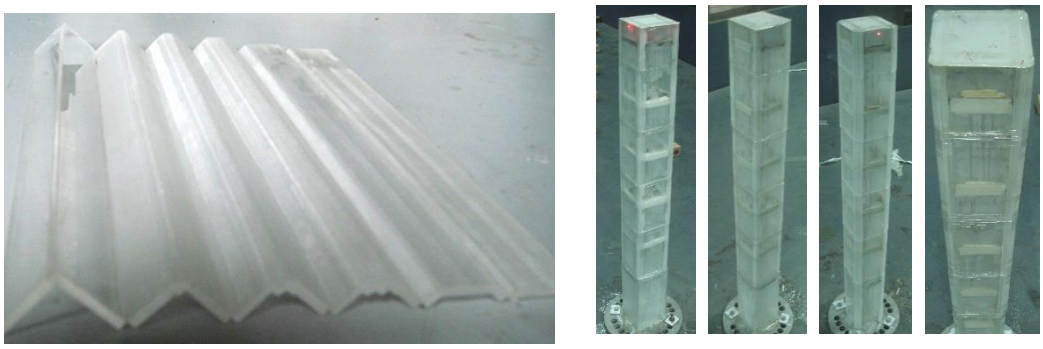


Figure 4. Some photos of the MDOF model and coated strips for adjusting the chamfer ratio.

Table 1 shows the structural parameters of different chamfer models. In Table 1, n_0 is the primary frequency of each model, M is equivalent mass, ξ is structural damping ratio, Sc is Scruton number, and R_c is the chamfer ratio. As seen from Figure 4 and Table 1, the cross-sectional shapes of each model are smooth from top to bottom and the structural parameters of each model have little difference, which indicates that the above method of adjusting the chamfer ratio is satisfactory. As the structural parameters of all these test cases are the nearly same except the chamfer ratio, it can be reasonably stated that the difference in wind-induced vibration between these cases was caused by the differences in chamfer ratio.

Table 1. The structural parameters of models with different chamfer ratio.

Case	n_0	M	ξ	Sc	R_c
1	9.9 Hz	2.1 kg/m	2.4%	8.1	0%
2	9.6 Hz	2.2 kg/m	2.3%	8.0	2.5%
3	9.6 Hz	2.2 kg/m	2.2%	7.8	5%
4	9.2 Hz	2.1 kg/m	2.4%	7.9	7.5%
5	9.2 Hz	2.0 kg/m	2.6%	8.3	12.5%

The generalized mass (M) and Scruton number (Sc) can be expressed by Equations (1) and (2), respectively.

$$M = \frac{\int_0^H m(z)\phi^2(z)d_z}{\int_0^H \phi^2(z)d_z} \quad (1)$$

$$Sc = \frac{2M\xi_s}{\rho_a D^2} \quad (2)$$

where $m(z)$ and $\phi(z)$ are the mass per unit length and the mode shape of the model, respectively; H is the height of the model; ρ_a is the air density, and D is the width of the model.

The dynamic parameters in Table 1 are determined by the free vibration of MDOF models. Take Case 1 as an example: Figure 5a shows the time history of free vibration displacement obtained by a repeated hammering test. The attenuation time histories of other cases can be obtained by the same method. The time histories of normalized free vibration displacement are shown in Figure 5b and the PSD of free vibration displacement is shown in Figure 5c, where σ_y is the RMS displacement. As seen from Figure 5, the free vibration attenuation results of the aeroelastic model are very stable and satisfactory, and the free vibration results of each case are very close.

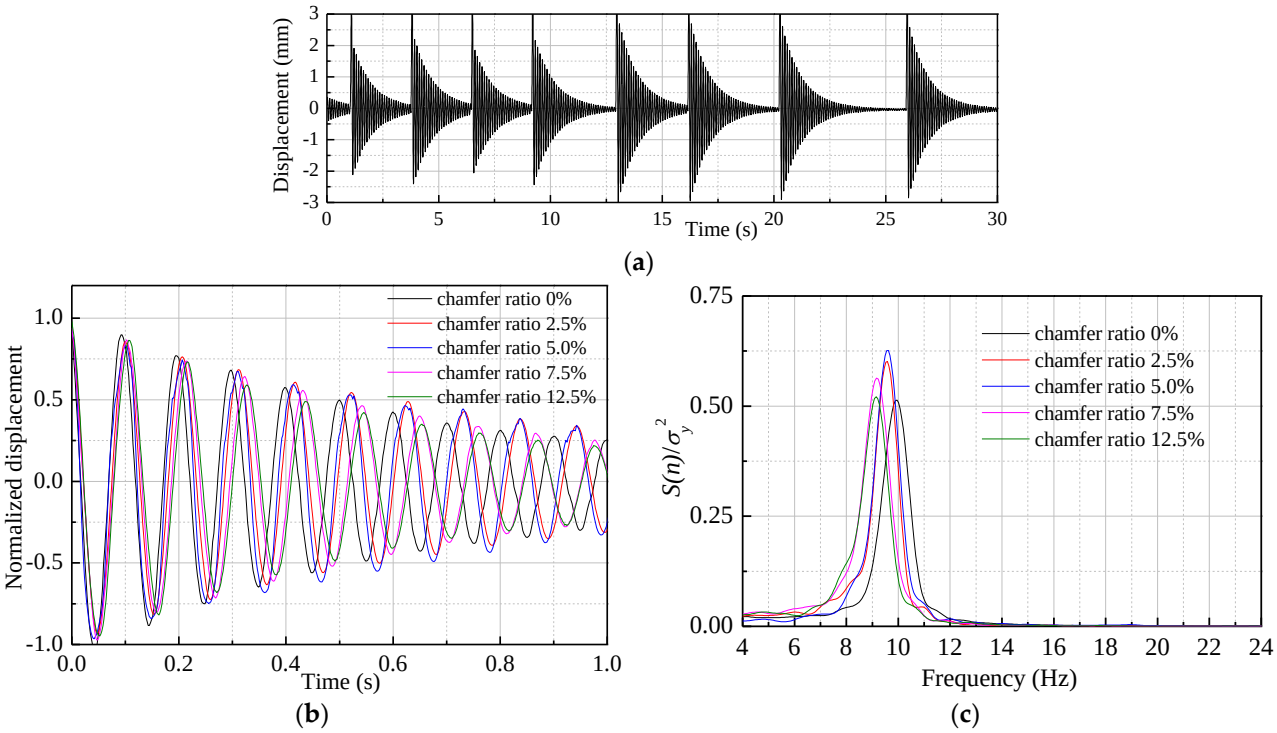


Figure 5. Free vibration result of the aeroelastic models with chamfered corners: (**a**) free vibration displacement of Case 2; (**b**) normalized free vibration displacement; (**c**) normalized PSD of free vibration displacement.

4. Wind-Induced Response of Aeroelastic Model with Chamfered Corner

Figure 6a shows the crosswind displacement of aeroelastic models with different chamfer ratios, where D is the cross-sectional width of the aeroelastic model, and σ_y/D is a percent sense. V_r is defined in Equation (3) as the reduced wind speed calculated by the wind speed at the top of the model. Since the structural parameters of each chamfer model are almost the same, the difference in test results of each model can be undoubtedly attributed to the effect of the chamfered corner.

$$V_r = \frac{V}{n_1 D} \tag{3}$$

where V, n_1, and D denote mean wind velocity, system vibration frequency in the first mode, and width of the model's windward side, respectively.

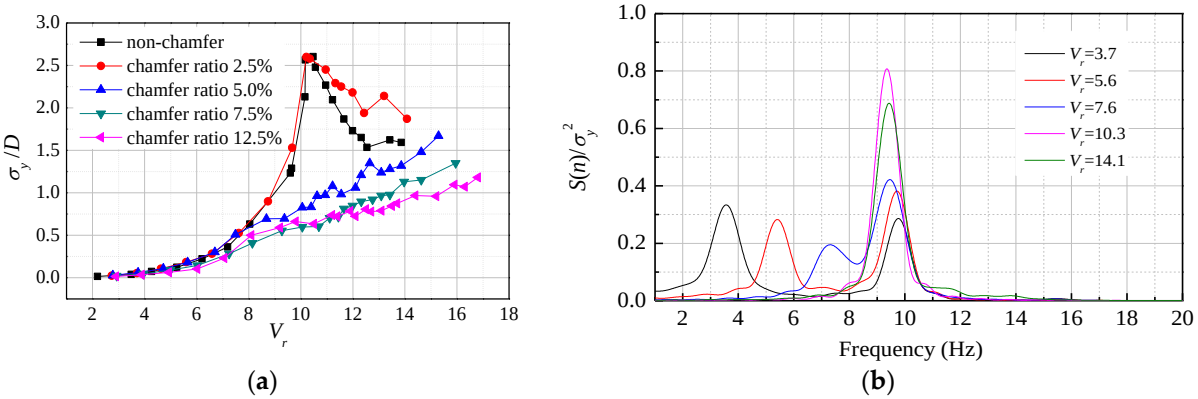


Figure 6. Crosswind responses and the normalized PSD of models with different chamfer ratios: (**a**) RMS responses; (**b**) normalized PSD of crosswind response.

As seen from Figure 6a, the RMS displacement of the non-chamfer model is the largest when V_r is close to the critical wind speed of VIV (V_c, in short, which can be calculated by the St number of existing studies shown in Figure 7—V_r corresponding to the maximum VIV displacement will be slightly larger than that calculated by St, but they are all called V_c in this paper for the sake of description). The displacement of the aeroelastic model with a 2.5% chamfer ratio is close to that of the non-chamfer model, which shows that reducing the chamfer ratio to 2.5% has an insignificant effect on VIV. However, when the chamfer ratio is increased to 5%, the crosswind displacement decreases significantly (especially when V_r is close to V_c), and the reduction of VIV response reaches 60%, where the reduction of VIV is computed by comparing experimental RMS displacement when V_r is close to V_c. The above results show that the chamfer ratio above 5% has a remarkable effect on suppressing the VIV of super high-rise buildings with square sections. It should be pointed out that the RMS response of the model with the chamfer ratio 2.5% is much larger than that of the non-chamfer case with an unknown reason when the wind speed is larger than VIV wind speed. This phenomenon was not explained in this paper; it may be caused by the dispersion of test data.

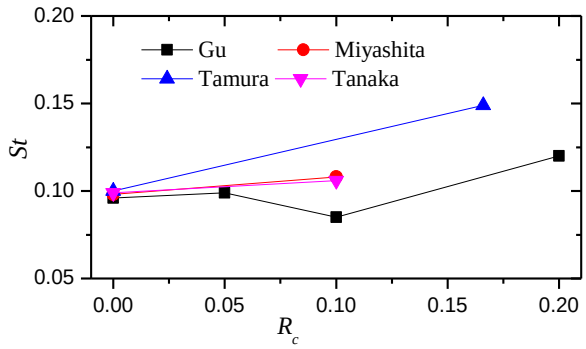


Figure 7. *St* number of chamfer model by existing studies [3,17,18,20].

Take Case 1 as an example. Figure 6b shows the normalized PSD of crosswind displacement. As can be seen, there are three spectral peaks in Figure 6b, corresponding to vortex shedding frequency, first-order frequency, and second-order frequency of the aeroelastic model, respectively, where the spectral peak corresponding to second-order frequency is very insignificant. With the increase of wind speed, the spectral peak frequency related to vortex shedding increases correspondingly, and its contribution decreases rapidly. According to the spectral peak position, the first-order frequency of the model is about 10 Hz and the second-order frequency is about 32 Hz. By calculating the band area of the power spectrum corresponding to the first and second-order frequency, respectively, it was found that the contribution of the second-order vibration is less than 1% when the test wind speed is close to VIV wind speed. When the reduced wind speed increases to about 10, the wind-induced vibration is dominated by the first-order vibration. Compared with the contribution of the first-mode vibration, the contribution of the second-order vibration is insignificant.

5. A Brief Analysis of the VIV Reduction Mechanism

As mentioned above, many researchers have studied the wind load of super high-rise buildings with different chamfer ratios based on synchronous pressure tests and high-frequency force balance tests. This paper does not repeat such tests but uses previous test data to assist the analysis of this study. Figure 8 shows the comparison between the crosswind base bending moment of the static model and the wind-induced response of the aeroelastic model in this paper, in which the base bending moment is obtained by Zhang through the force balance test [19]. The data in Figure 8 are normalized results, i.e., both the wind-induced bending moment and displacement of the non-chamfer are set to 1.

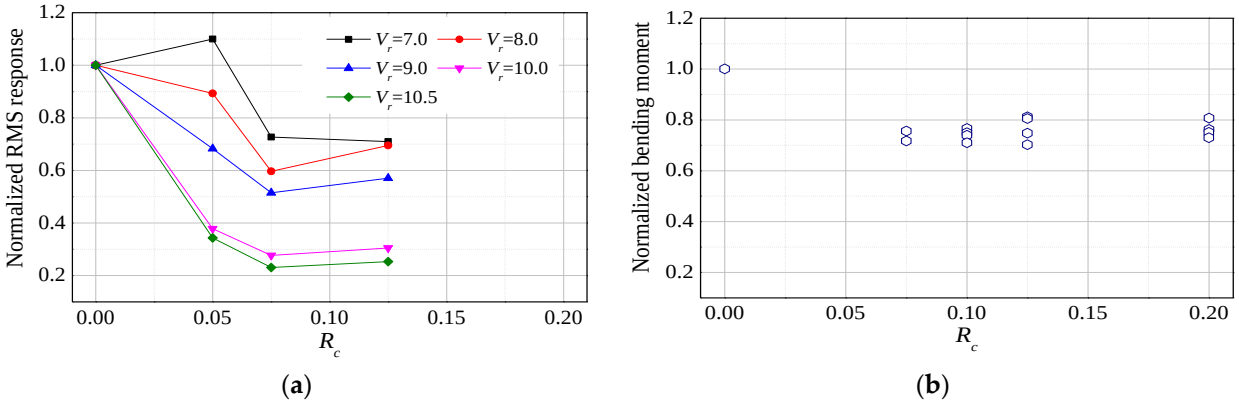


Figure 8. Normalized wind-induced response and bending moment: (**a**) normalized RMS responses; (**b**) normalized bending moment [19].

It can be seen from Figure 8 that:

(a) When V_r is smaller than V_c (V_r = 7.0, V_r = 8.0, etc.), the normalized wind-induced response is consistent with the results of the normalized bending moment, and both of them gradually decrease with the increase in chamfer ratio. When the chamfer ratio reaches 7.5%, the normalized bending moment and wind-induced response reach the minimum, and the decrease is about 25% compared to the non-chamfer model;

(b) When V_r is close to V_c (V_r = 10.0, V_r = 10.5, etc.), the normalized wind-induced response is very different from the normalized bending moment. With the increase of the chamfer ratio, the wind-induced response decreases significantly faster than that of the base bending moment. When the chamfer ratio is equal to 7.5%, the decrease of wind-induced response reaches 70%, which is much greater than that of base bending moment (25%);

(c) The vibration reduction effect is not always positively correlated with the chamfer ratio. When the chamfer ratio is larger than 7.5% (R_c = 10%, R_c = 12.5%, etc.), the normalized wind load and response rebound to some extent.

In order to analyze the VIV reduction mechanism from the perspective of aeroelastic effects, the aerodynamic damping ratio of the aeroelastic model is calculated by using the random decrement technique. The random decrement technique is widely used to evaluate aerodynamic damping ratios from random vibration responses of structures [27–29]. In the process of the random decrement technique used in this paper, the bandwidth band pass filter is [n_1(1 − 20%), n_1(1 + 20%)], and the time length of the data sample is 100 s. The amplitude of the signal interception is σ_y with an error range of 5%. On the basis of the random decrement technique, free attenuation curves can be obtained through time histories of tip displacement. The exponential decay rate (total damping (ξ_t)) could be identified by the envelope of random decrement signatures, and the aerodynamic damping ratio (ξ_a) could then be calculated by Equation (4).

$$\xi_a = \xi_t - \xi_s \tag{4}$$

where the subscript a, t, and s denote aerodynamic, total, and structural, respectively.

Figure 9 shows the aerodynamic damping results of the models with different chamfer ratios. It can be seen from Figure 9 that:

(a) When the chamfer ratio is 2.5%, the aerodynamic damping is consistent with that of the non-chamfer model, and there is a significant negative aerodynamic damping phenomenon when V_r is close to V_c.

(b) When the chamfer ratio increases to 5%, the negative aerodynamic damping phenomenon disappears. Obviously, this result of the aerodynamic damping ratio is closely related to the wind-induced response.

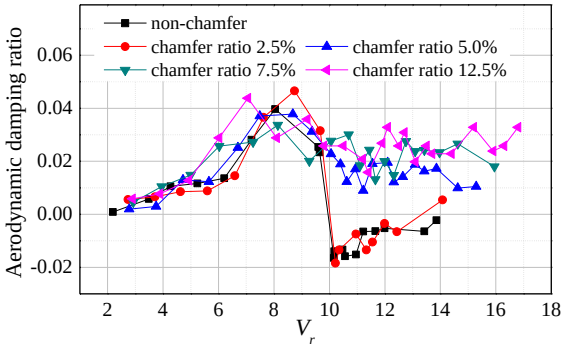


Figure 9. Aerodynamic damping ratio of the aeroelastic model with different chamfer ratios.

The above analysis shows that the reduction of crosswind response is mainly caused by the reduction of wind load when the V_r is small. However, when V_r is close to V_c, the reduction of the VIV response is affected not only by the wind load but also by the aeroelastic effect significantly. The wind load here means the aerodynamic force on the static model.

Based on the above results, the following conclusion can be drawn: a chamfer ratio of greater than 5% will significantly reduce the wind-induced response of a tall building with a square section, and the best modification effect can be achieved with the chamfer ratio of about 7.5%, because this chamfer ratio can significantly reduce the crosswind response, especially the VIV response.

6. Reduction Effect of Rounded Corners on VIV

Aeroelastic Model with Rounded Corners

Figure 10 shows the cross-sectional diagram of the rounded-corner models, and Figure 11 shows some photos of the rounded model. The rounded ratio is 0%, 12.5%, 15%, and 17.5% sequentially, and is defined as the ratio of the rounded size of one corner to the cross-sectional width. Table 2 shows the structural parameters of each test case; as seen in Table 2, the structural parameters of each model have little difference.

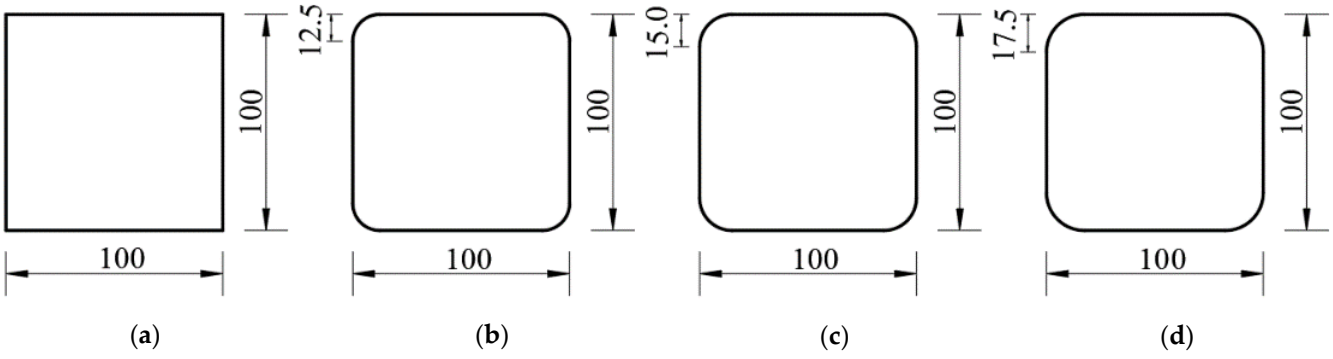


Figure 10. Sections of MDOF model with rounded corner (unit: mm): (**a**) rounded ratio 0%; (**b**) rounded ratio 2.5%; (**c**) rounded ratio 5%; (**d**) rounded ratio 7.5%.



Figure 11. Some photos of the MDOF model with rounded corners.

Table 2. The structural parameter of rounded-corner models.

Case	n_1	M	ξ	Sc	R_r
1	9.94 Hz	2.1 kg/m	2.4%	8.1	0%
2	9.62 Hz	2.0 kg/m	2.7%	8.4	12.5%
3	9.30 Hz	1.9 kg/m	2.7%	8.2	15.0%
4	9.60 Hz	1.9 kg/m	2.5%	7.5	17.5%

The dynamic parameters in Table 2 were determined by free vibration and the wind-induced vibration of MDOF models.

7. Wind-Induced Response of Aeroelastic Model with Rounded Corners

Figure 12 shows the RMS crosswind displacement of aeroelastic models with different rounded ratios, where σ_y/D is a percent sense. As can be seen from Figure 12, the result of this study is similar to the result of Kawai [13]. The rounded corner can significantly reduce the crosswind displacement. When the rounded ratio is about 12.5%, the VIV response is significantly suppressed, and the response amplitude is reduced by about 50%. When the rounded ratio is increased to 15%, the VIV response decreases more significantly, and the response amplitude is reduced by about 70%. It should be noted that the Reynolds number effect may be significant for rounded models. As seen from Figures 12 and 13, the *St* number increases with the increase of the rounded ratio to some extent. The change in *St* number is not very significant according to the result of Figure 13 by Hayashide [14], which indicates that the influence of the Reynolds number effect on wind-induced response is limited to some extent when the rounded ratio is smaller than 25%. Further relevant research about this problem is necessary.

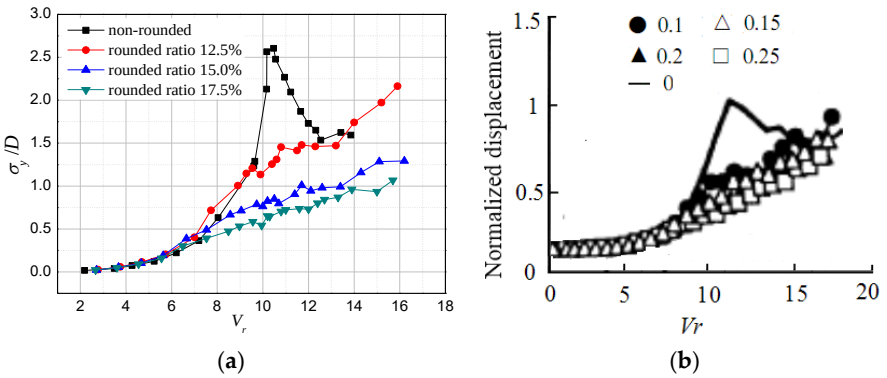


Figure 12. Crosswind responses of models with different rounded ratios: (**a**) RMS responses of this study; (**b**) RMS responses of SDOF model result [13].

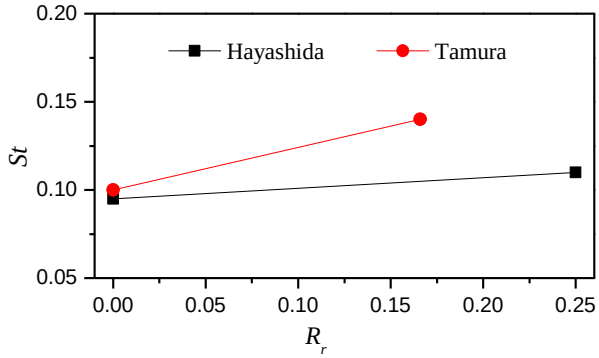


Figure 13. *St* number of rounded model by existing studies [14,20].

8. A Brief Analysis of the VIV Reduction Mechanism

Because a large number of researchers have studied the wind load of super high-rise buildings with different rounded corners based on rigid pressure models and force balance tests, this paper does not repeat such tests but uses the existing test data to assist the analysis. Figure 14 shows the comparison between the wind-induced response in this paper and the base bending moment in the existing reference [19]. As seen from Figure 14, the reduction of the base moment is not obvious when the rounded ratio is less than 12.5%, while the reduction of the base moment becomes quite significant when the rounded ratio increases to 15%. This phenomenon is similar to the wind response results of the aeroelastic model at small reduced wind speeds (V_r = 6, V_r = 7, etc.). However, when V_r is close to V_c (V_r = 10, V_r = 10.5, etc.), the response of each rounded model decreases; especially after the rounded ratio increases to 15%, the crosswind response decreases significantly, and the decrease of wind-induced response is more significant than that of the base bending moment.

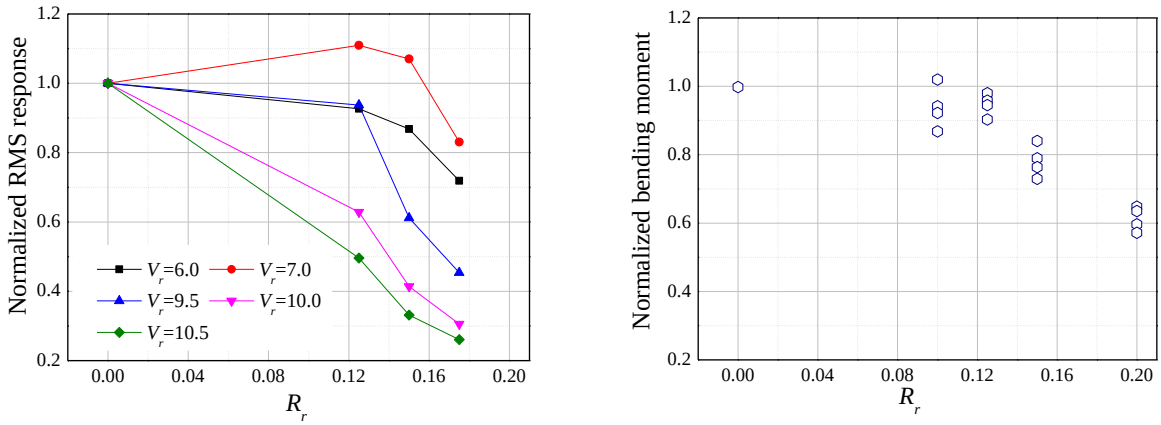


Figure 14. Comparison between the result of this paper and that of Zhang's [19].

Figure 15 shows the aerodynamic damping ratio of the models with different rounded ratios. It can be seen from Figure 15 that when the rounded ratio is 12.5%, the negative aerodynamic damping phenomenon near the VIV wind speed ceases to exist, and the aerodynamic damping ratio becomes positive at high wind speed. This phenomenon is more obvious when the rounded ratio increases to 15%. As is well known, the aerodynamic damping ratio must be dependent on the vibration amplitude; in other words, these characteristics of aerodynamic damping and wind-induced response are mutually causal.

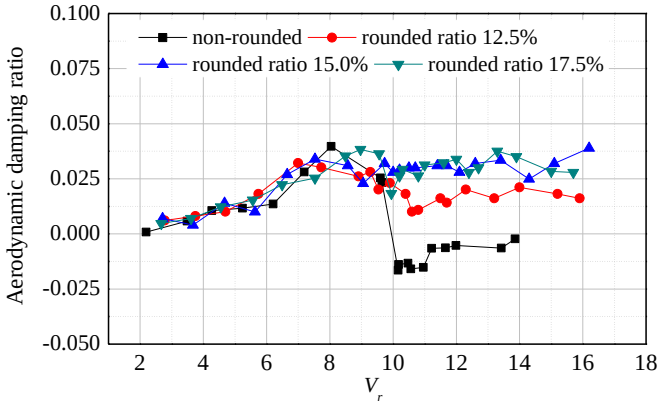


Figure 15. Aerodynamic damping ratio of the aeroelastic model with different rounded ratios.

The above analysis indicates that the rounded corner not only reduces the wind load but also improves the aeroelastic effect significantly. Generally speaking, when the rounded ratio reaches 15%, the crosswind vibration of super high-rise buildings can be effectively suppressed.

9. Conclusions

(1) The chamfer corner can significantly reduce the crosswind response of super high-rise buildings. A chamfer ratio greater than 5% will significantly reduce the wind-induced response of a tall building with a square section, and when the chamfer ratio is increased to about 7.5%, the modification effect is the best with about a 60% reduction of VIV response. However, an excessive chamfer ratio cannot further increase the modification effect.

(2) The rounded corners can also significantly reduce the crosswind response of super high-rise buildings. When the rounded ratio is not greater than 12.5%, the crosswind response at a small wind speed is not significantly reduced, but the response at the critical wind speed of VIV is effectively controlled. A rounded ratio of more than 15% is recommended to suppress the crosswind vibration of super high-rise buildings, which could reduce the VIV response by 70%.

(3) When the reduced wind speed is small, the reduction of the crosswind response of chamfered and rounded models is mainly caused by the reduction of wind load, while when the reduced wind speed approaches the critical wind speed of VIV, the reduction of the VIV response of the chamfer model is mainly caused by the aeroelastic effects of different shapes.

Author Contributions: Conceptualization, L.W.; Writing – original draft, W.Z. All authors have read and agreed to the published version of the manuscript.

Funding: This research was funded by National Natural Science Foundation of China: 51708186.

Institutional Review Board Statement: Not applicable.

Informed Consent Statement: Not applicable.

Conflicts of Interest: The authors declare no conflict of interest.

References

1. Quan, Y.; Gu, M. Across-wind equivalent static wind loads and responses of super-high-rise buildings. *Adv. Struct. Eng.* **2012**, *15*, 2145–2155. [CrossRef]
2. Wang, L.; Zhang, W.; Liu, L.S.; Zhang, Z.H. Wind force of super high-rise buildings with hexagonal section. *Structures* **2021**, *33*, 283–291. [CrossRef]
3. Gu, M.; Cao, H.L.; Quan, Y. Experimental study of across-wind aerodynamic damping of super high-rise buildings with aerodynamically modified square cross-sections. *Struct. Design Tall Spec. Build.* **2014**, *23*, 1225–1245. [CrossRef]
4. Wang, L.; Wang, Z.; Huang, N.; Fan, X.-Y.; Zhang, Z. Comparative analysis of cross-wind load code for high structures with circular sections. *Structures* **2021**, *43*, 1177–1186. [CrossRef]

5. Watanabe, Y.; Isyumov, N.; Davenport, A. Empirical aerodynamic damping function for tall buildings. *J. Wind Eng. Ind. Aerodyn.* **1997**, *72*, 313–321. [CrossRef]
6. Huang, P.; Quan, Y.; Gu, M. Experimental study of aerodynamic damping of typical tall buildings. *Math. Probl. Eng.* **2013**, *2013*, 731572. [CrossRef]
7. Li, S.Y.; Xiao, C.Y.; Fan, Y.G.; Chen, Z.-Q. Experimental investigation of aerodynamic damping on super-high-rise buildings with square cross section under the action of full-direction wind. *J. Hunan Univ.* **2015**, *42*, 9–15.
8. Liu, T.; Zhang, W.; Yue, Q. A study on vortex-induced vibration of supertall buildings in acrosswind. *Struct. Des. Tall Spec. Build.* **2011**, *20*, 902–910. [CrossRef]
9. Wang, L.; Liang, S.; Huang, G.; Song, J.; Zou, L. Investigation on the unstability of vortex induced resonance of high-rise buildings. *J. Wind Eng. Ind. Aerodyn.* **2018**, *175*, 17–31. [CrossRef]
10. Wang, L.; Fan, X.Y.; Liang, S.G.; Song, J.; Wang, Z.K. Improved expression for across-wind aerodynamic damping ratios of super high-rise buildings. *J. Wind Eng. Ind. Aerodyn.* **2018**, *176*, 263–272. [CrossRef]
11. Liang, S.; Yang, W.; Song, J.; Wang, L.; Hu, G. Wind-induced responses of a tall chimney by aeroelastic wind tunnel test using a continuous model. *Eng. Struct.* **2018**, *176*, 871–880. [CrossRef]
12. Kwok, K.; Wilhelm, P.; Wilkie, B. Effect of edge configuration on wind-induced response of tall buildings. *Eng. Struct.* **1988**, *10*, 135–140. [CrossRef]
13. Kawai, H. Effect of corner modifications on aero-elastic instabilities of tall buildings. *J. Wind Eng. Ind. Aerodyn.* **1998**, *74–76*, 719–729. [CrossRef]
14. Hayashida, H.; Iwasa, Y. Aerodynamic shape effects of tall building for vortex induced vibration. *J. Wind Eng. Ind. Aerodyn.* **1990**, *33*, 237–242. [CrossRef]
15. Hayashida, H.; Mataki, Y.; Iwasa, Y. Aerodynamic damping effects of tall building for a vortex induced vibration. *J. Wind Eng. Ind. Aerodyn.* **1992**, *43*, 1973–1983. [CrossRef]
16. Gu, M.; Quan, Y. Across-wind loads of typical tall buildings. *J. Wind Eng. Ind. Aerodyn.* **2004**, *92*, 1147–1165. [CrossRef]
17. Miyashita, K.; Ohkuma, T.; Tamura, Y. Wind-induced response of high-rise buildings. *J. Wind Eng. Ind. Aerodyn.* **1993**, *50*, 319–328. [CrossRef]
18. Tanaka, H.; Tamura, Y.; Ohtake, K.; Nakai, M.; Kim, Y.C. Experimental investigation of aerodynamic forces and wind pressures acting on tall buildings with various unconventional configurations. *J. Wind Eng. Ind. Aerodyn.* **2012**, *107–108*, 179–191. [CrossRef]
19. Zhang, Z.; Quan, Y.; Gu, M.; Xiong, Y. Effects of corner chamfering and rounding modification on aerodynamic coefficients of square tall buildings. *China Civ. Eng. J.* **2013**, *46*, 12–20.
20. Tamura, Y.; Xu, X.D.; Tanaka, H. Aerodynamic and Pedestrian-Level Wind Characteristics of Super-Tall Buildings with Various Configurations. *Procedia Eng.* **2017**, *199*, 28–37. [CrossRef]
21. Kim, Y.M.; You, K.P.; Ko, N.H. Across-wind responses of an aeroelastic tapered tall building. *J. Wind Eng. Ind. Aerodyn.* **2008**, *96*, 1307–1319. [CrossRef]
22. Kim, Y.; Bandi, E.; Yoshida, A.; Tamura, Y. Response characteristics of super-tall buildings–Effects of number of sides and helical angle. *J. Wind Eng. Ind. Aerodyn.* **2015**, *145*, 252–262. [CrossRef]
23. Hu, G.; Hassanli, S.; Kwok, K.C.S.; Tse, K.T. Wind-induced responses of a tall building with a double-skin façade system. *J. Wind Eng. Ind. Aerodyn.* **2017**, *168*, 91–100. [CrossRef]
24. Tse, K.T.; Hu, G.; Song, J.; Park, H.S.; Kim, B. Effects of corner modifications on wind loads and local pressures on walls of tall buildings. *Build. Simul.* **2020**, *14*, 1109–1126. [CrossRef]
25. Hu, J.C.; Zhou, Y.; Dalton, C. Effects of the corner radius on the near wake of a square prism. *Exp. Fluids* **2006**, *40*, 106–118. [CrossRef]
26. *GB50009-2012*; Load Code for the Design of Building Structures. China Architecture and Building Press: Beijing, China, 2012.
27. Kareem, A.; Gurley, K. Damping in structures: Its evaluation and treatment of uncertainty. *J. Wind Eng. Ind. Aerodyn.* **1996**, *59*, 131–157. [CrossRef]
28. Marukawa, H.; Kato, N.; Fujii, K.; Tamura, Y. Experimental evaluation of aerodynamic damping of tall buildings. *J. Wind Eng. Ind. Aerodyn.* **1996**, *59*, 177–190. [CrossRef]
29. Tamura, Y.; Suganuma, S.Y. Evaluation of amplitude-dependent damping and natural frequency of buildings during strong winds. *J. Wind Eng. Ind. Aerodyn.* **1996**, *59*, 115–130. [CrossRef]

Disclaimer/Publisher's Note: The statements, opinions and data contained in all publications are solely those of the individual author(s) and contributor(s) and not of MDPI and/or the editor(s). MDPI and/or the editor(s) disclaim responsibility for any injury to people or property resulting from any ideas, methods, instructions or products referred to in the content.